CHARACTERIZATION OF THE IPNS RADIATION EFFECTS MODULE

Bradley J. Micklich[1], Erik B. Iverson[2], Michael Wohlmuther[3] and Franz X. Gallmeier[2]

[1]*Argonne National Laboratory , 9700 S. Cass Ave., Argonne, IL USA, bjmicklich@anl.gov*
[2]*Oak Ridge National Laboratory, Oak Ridge, TN USA*
[3]*Paul Scherrer Institute, Villigen, Switzerland*

The radiation effects module (REM) at Argonne's Intense Pulsed Neutron Source has been used for a wide variety of irradiation experiments over the facility's lifetime. Recently planned and executed experiments include studies of radiation damage in optical fibers and scintillators for use in high-energy physics detectors, irradiation of optical components for SNS neutron scattering instruments, irradiation of dilute fissile mixtures to study separations processes, and irradiation of foils and wires for neutronic characterization of the facility. Characterization of the neutron flux profile in the REM is essential for planning experiments and analyzing the resulting data. In this paper we compare the neutron fluxes obtained from recent MCNPX calculations with the results of previous experiments which used a set of activation foils to measure the neutron flux from high energies down to thermal at two locations in the REM. We also compare recent activation measurements in nickel and bismuth samples with predictions using the CINDER90 code and neutron fluxes generated using MCNPX.

I. INTRODUCTION

The Intense Pulsed Neutron Source (IPNS) is a US Department of Energy user facility for materials science research located at Argonne National Laboratory. The IPNS produces neutrons by directing 450-MeV protons onto a depleted uranium target at a nominal beam current of 15 μA. One of the experimental facilities at IPNS is the radiation effects module (also called the REM). This facility is a vertical fast flux irradiation tube with inner diameter about 4.12 cm that extends about 4 meters down into the shielding surrounding the target, with the bottom of the tube being about 7.5 cm lower than the target horizontal centerline. The bottom of the REM is in the outer reflector of the target/moderator/reflector system. Samples for irradiation are inserted into the tube from on top of the shielding monolith. The sample volume is pumped down to rough vacuum, but no provisions are made for electrical or other connections to be used for temperature measurement and control or for remote data readout.

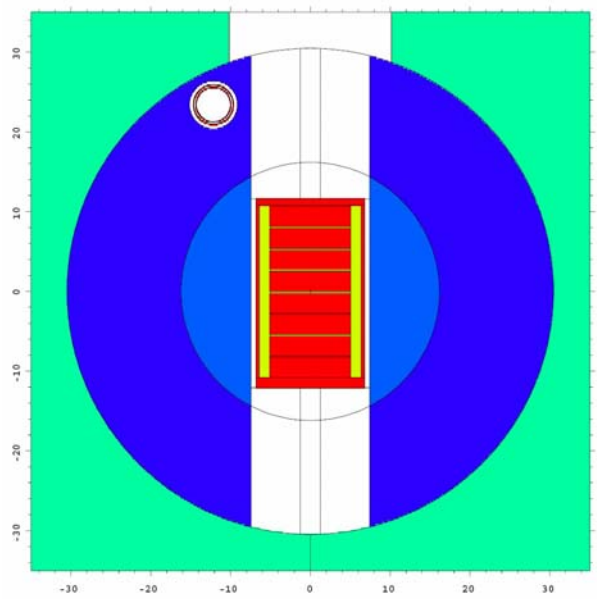

Figure 1. MCNPX model of the IPNS target and reflector region in the plane of the target centerline. The REM is in the upper left of the figure. Protons are incident from the top. Dimensions are in centimeters.

The REM has been used for a wide variety of irradiation experiments over the facility's lifetime. Recently planned and executed experiments include studies of radiation damage in optical fibers and scintillators for use in high-energy physics detectors, irradiation of optical components for SNS neutron scattering instruments, irradiation of dilute fissile mixtures to study separations processes, and irradiation of foils and wires for neutronic characterization of the facility. Characterization of the neutron flux profile in the REM is essential for planning experiments and analyzing the resulting data.

In this paper we compare the neutron fluxes obtained from recent MCNPX calculations with the results of previous activation foil measurements of the neutron flux

from high energies down to thermal at two positions in the REM. We also compare recent activation measurements in nickel and bismuth samples with predictions using the CINDER'90 [1] code and neutron fluxes generated using MCNPX [2]. As the cross section data used in estimating reaction products are critical to this exercise, we offer comments on the dosimetry cross sections available for use in the present work.

II. MONTE CARLO SIMULATIONS

Radiation transport codes such as MCNPX are often used to simulate the results of experiments, so it is useful to benchmark the results of simulations against measurements wherever possible. MCNPX 2.5.0 was used to calculate the neutron flux in the REM as a function of height for the nominal IPNS beam current of 15 μA. The vertical profiles of the fast (E_n > 0.1 MeV) and thermal (E_n < 0.1 eV) fluxes are shown in Figure 2. The fast flux exhibits a peak at the target centerline. The thermal flux peaks at the bottom of the REM (next to the outer reflector at this point), drops rapidly with height, and shows a flattened profile at the transition out of the reflector.

The neutron energy spectrum has been measured with activation foils on several occasions. The most complete set of measurements is that of Greenwood [3]. These measurements were made at a time when IPNS was run using an enriched uranium target that contained 77% ^{235}U, unlike the 0.2% ^{235}U in the present (depleted uranium) target. Packets containing iron, titanium, cobalt, gold, lutetium, aluminum, indium, manganese, copper, and niobium foils were used to determine the neutron energy spectrum at two locations: at the target centerline (about 7.5 cm above the bottom of the REM) and at another location about 30 cm higher. Figure 3 compares the measured fluxes to the results of the MCNPX calculation. At both positions, the calculated neutron energy spectrum is larger than the measured spectrum by a factor of 2-4 over the entire energy range from the highest energies down to thermal. Note that for E_n > 10 MeV, the simulated neutron flux is the same for the booster target and the depleted uranium target, since these neutrons come from the intranuclear cascade in the uranium and thus do not depend on uranium enrichment, as do fission neutrons. The structure that is present in the measurement but not in the calculation is likely the result of artifacts in the unfolding procedure, whereby the unfolded spectrum takes on the assumed spectral shape in each energy range.

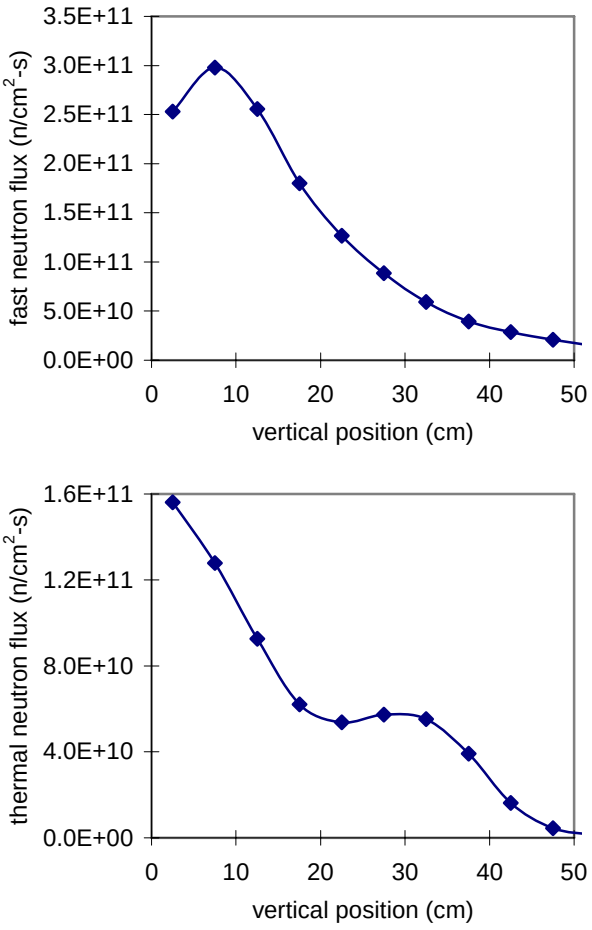

Figure 2. Profiles of fast (top) and thermal (bottom) flux as a function of height in the REM tube from MCNPX simulation.

III. NICKEL WIRE MEASUREMENTS

III.A. Nickel Dosimetry Cross Sections

Nickel is an element frequently used in spectral measurements as the natural element is readily obtained in high purity and has reactions with both fast and thermal neutrons for which the products have easily counted gamma rays. As such, nickel cross sections have been extensively studied for their use in dosimetry. The primary reactions used are ^{58}Ni(n,p)^{58}Co, ^{58}Ni(n,2n)^{57}Ni, and ^{64}Ni(n,γ)^{65}Ni. The first two of these are induced by fast neutrons and the third by thermal neutrons. The half-lives and principal emission gamma rays from the products of these reactions are listed in Table 1 [4,5].

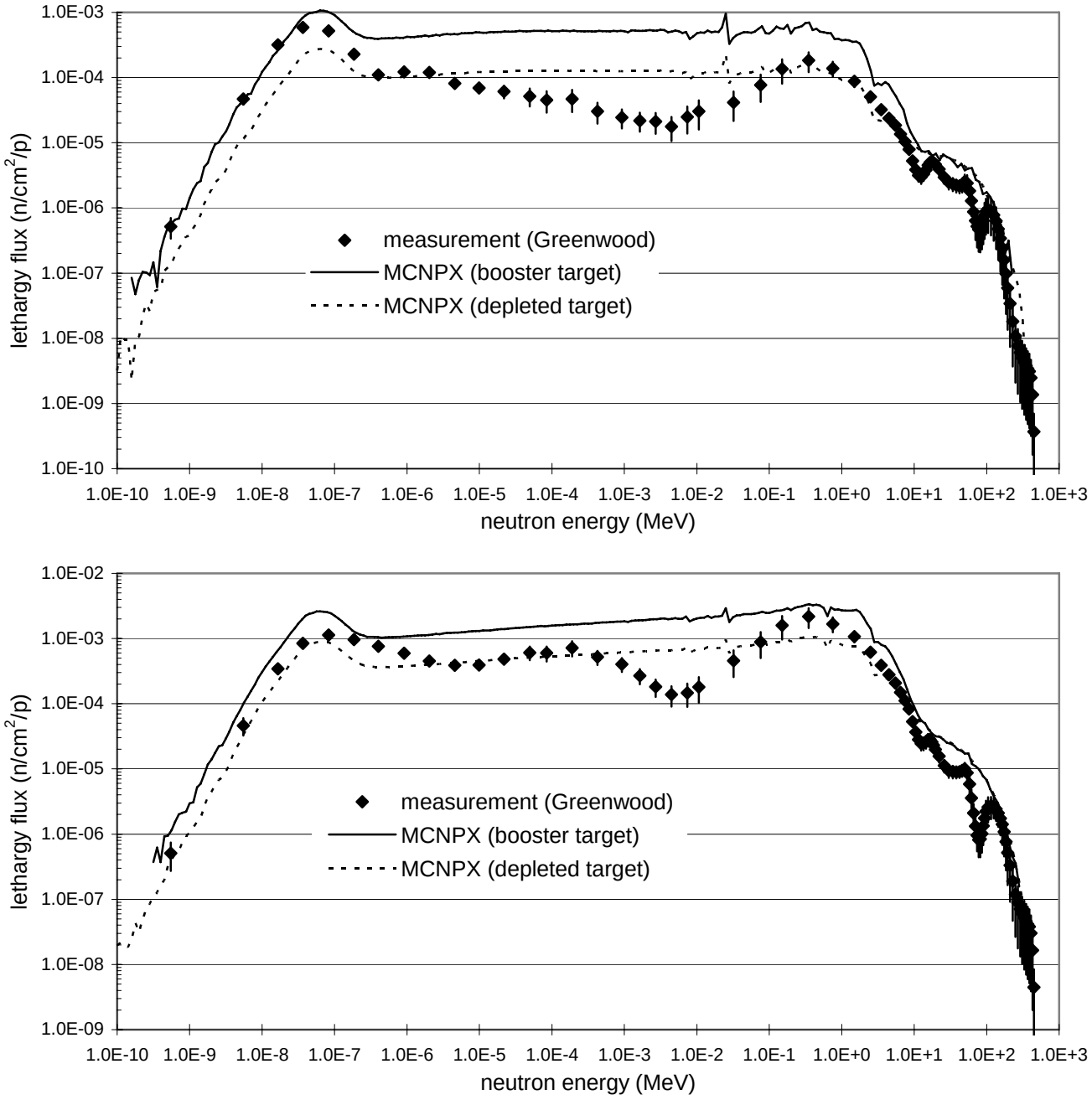

Figure 3. Comparison of measured and simulated neutron fluxes at the upper (top) and lower (bottom) measurement positions from the foil-based neutron flux measurement of Greenwood [3].

TABLE I. Half lives and principal gamma emissions from products of n+Ni reactions.

Reaction Product	Half-life	Principal Gamma Energies (keV)
^{58}Co	70.88 d	810.8
^{58m}Co	9.1 h	24.9
^{57}Ni	35.6 h	1377.6
^{65}Ni	2.517 h	1481.9, 1115.5

The radionuclide ^{58}Co is produced by the reaction ^{58}Ni(n,p) to both the ground state and an excited (metastable) state. The ground state has a half-life of 70.88 d, and the metastable state has a half-life of 9.1 hrs. The metastable state decays directly to the ground state, but emits only low-energy gamma rays which are difficult to count. The ground state emits a 810.8-keV gamma ray in 99.43% of decays.

As a result, the most practical means of determining the initial populations of the ground and metastable states after irradiation is to count the samples twice, once immediately after irradiation and again two or three days later, after the excited state has essentially completely decayed to the ground state. Because of the relative lengths of the half-lives, the activity of the 810.8-keV gamma will initially increase before slowly decreasing.

After an irradiation time T, the populations of the metastable and ground states are given by

$$N_{m0} = \frac{S_m}{\lambda m}\left(1 - e^{-\lambda_m T}\right) \qquad (1)$$

$$N_{g0} = \frac{S_g}{\lambda_g}\left(1 - e^{-\lambda_g T}\right) + \frac{S_m}{\lambda_g} \times \left(1 + \frac{\lambda_g}{\lambda_m - \lambda_g} e^{-\lambda_m T} - \frac{\lambda_m}{\lambda_m - \lambda_g} e^{-\lambda_g T}\right) \qquad (2)$$

where S_m and S_g are the production rates for the two states and T is the length of the irradiation. After the end of irradiation, the populations of the two states are determined by this partially coupled set of equations

$$\frac{dN_m}{dt} = -\lambda_m N_m \qquad (3)$$

$$\frac{dN_g}{dt} = -\lambda_g N_g + \lambda_m N_m \qquad (4)$$

Solving for the number of ground state nuclei at time t (time after irradiation ceases), we find

$$N_g(t) = N_{g0} e^{-\lambda_g t} + \frac{\lambda_m N_{m0}}{\lambda_g - \lambda_m}\left(e^{-\lambda_m t} - e^{-\lambda_g t}\right) \qquad (5)$$

By counting the irradiated material at two different times, we can obtain two equations in the two unknowns N_{g0} and N_{m0} which can be solved to find the populations of the two states at the end of irradiation.

Cross sections for this reaction are shown in Figure 4. The cross sections from the ENDF libraries are pointwise and thus appear as curves, while the CINDER'90 cross sections are multigroup and are shown as histograms. The ^{58}Ni(n,p) cross section in the ENDF-based MCNPX transport libraries is the total (n,p) cross section, the sum of the partial cross sections to the ground and metastable states. This cross sections agrees well with that from the llldos dosimetry library used with MCNPX. The llldos library also has a separate cross section to the ground state of ^{58}Co, but this is just one-half of the total. This differs from the CINDER'90 cross section and does not reflect the results of recent measurements [6-8].

The cross sections in the International Reactor Dosimetry File (IRDF) go only to 20 MeV and report just the total (n,p) cross section. Note that the ENDF cross sections for this reaction are limited to a maximum E_n of 20 MeV, even for those data sets listed as having a maximum energy of 150 MeV. The CINDER library extends up to E_n = 25 MeV for all reactions. Production of residual nuclides at higher energies is calculated in MCNPX using model-based physics rather than cross section tables.

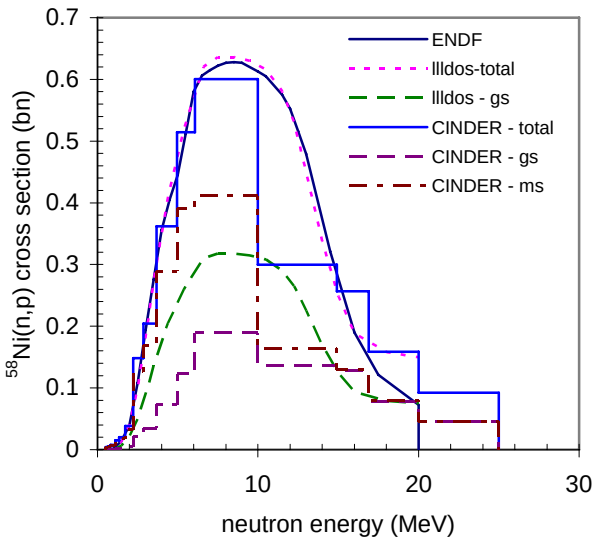

Fig. 4. Cross sections for ^{58}Ni(n,p)^{58}Co and ^{58}Ni(n,p)^{58m}Co reactions [gs = ground state, ms = metastable state].

Cross sections for the ^{58}Ni(n,2n)^{57}Ni reaction are shown in Figure 5. Again, the ENDF-based transport library and the llldos dosimetry library are in agreement for this cross section. The IRDF cross section is essentially that of ENDF. The CINDER'90 cross sections are somewhat higher than those in ENDF for E_n below 14 MeV and lower for energies between 14 and 20 MeV.

Cross sections for the ^{64}Ni(n,γ)^{65}Ni reaction are shown in Figure 6. The CINDER'90 cross sections agree well with the ENDF transport cross sections. However, the dosimetry cross section in llldos shows significant discrepancies from both.

III.B. Nickel Wire Measurements

We irradiated a 2-mm diameter, 50-cm long wire of 99.999% nickel in the REM for two hours at an average current of 15 μA to obtain a vertical profile of the fast and thermal neutron fluxes in the REM. After allowing for decay of short-lived activation products, the wire was cut into sections approximately 2.5 cm long. The gamma emissions were counted using a 50% HPGe detector and

the data analyzed using the Ortec GammaVision software package. Gamma rays were analyzed corresponding to the products of the ^{58}Ni(n,p)^{58}Co, ^{58}Ni(n,2n)^{57}Ni, and ^{64}Ni(n,γ)^{65}Ni reactions. The activities of these nuclides were calculated using the MCNPX and CINDER'90 codes as driven by a Perl script [9] which controls the activation calculation.

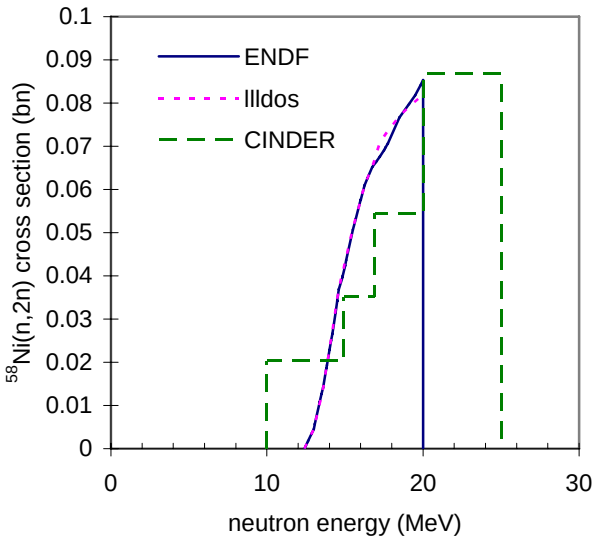

Fig. 5. Cross sections for ^{58}Ni(n,2n)^{57}Ni reaction.

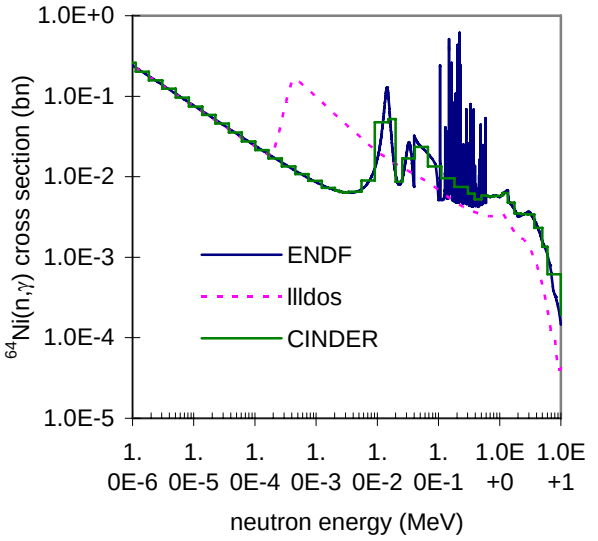

Fig. 6. Cross sections for ^{64}Ni(n,γ)^{65}Ni reaction.

The activity of the ground state of ^{58}Co was measured by counting the 810.8-keV gamma ray as described above. Because the wire segments were initially too hot to count, only some of the least activated segments could be counted early enough to get the early-time measurement described above. Therefore only for these two segments could we estimate the initial activities of both the ground and metastable states. Table II compares the measured and calculated activities. While the CINDER calculation predicts the activity of the ground state very well, it overpredicts the initial metastable state activity by 60-70%. For the remaining segments, we calculated the activity of the 810.8-keV gamma ray at the time each wire segment was counted. These calculated values are compared to the measurements in Figure 7. The simulations show a greater peak in the ^{58}Co activity at the midplane of the target than do the measurements. This corresponds to the peak in the fast flux seen in the MCNPX neutron fluxes above. The agreement at the upper end of the wire is quite good.

We also estimated the ^{58}Co activity at the two locations at which the Greenwood flux measurements were made. The Greenwood results for neutron flux using the enriched target were combined with an MCNPX estimate of the cross-section-weighted neutron flux ratio (enriched vs. depleted target) to derive the ^{58}Ni(n,p) reaction rates for the case of the depleted uranium target. For the lower foil packet location, this procedure results in a specific activity of about 5.0e+4 Bq/g at the time the corresponding wire segment was counted. This is still larger than the measured value of about 2.9e+4 Bq/g, but in better agreement than the value of 6.7e+4 Bq/g based on the neutron fluxes from MCNPX. At the location of the upper foil packet, the specific activity based on the Greenwood fluxes is about 3.9e+3 Bq/g compared to the experimental value of 6.0e+3 Bq/g and the MCNPX-derived value of 7.3e+3 Bq/g.

TABLE II. Initial activities for ^{58}Co and ^{58m}Co.

Wire segment	nuclide	Measured Activity (Bq)	Simulated Activity (Bq)
N18	^{58}Co	1.53e+3	1.07e+3
	^{58m}Co	1.67e+5	3.82e+5
N19	^{58}Co	1.10e+3	8.44e+2
	^{58m}Co	1.35e+5	3.00e+5

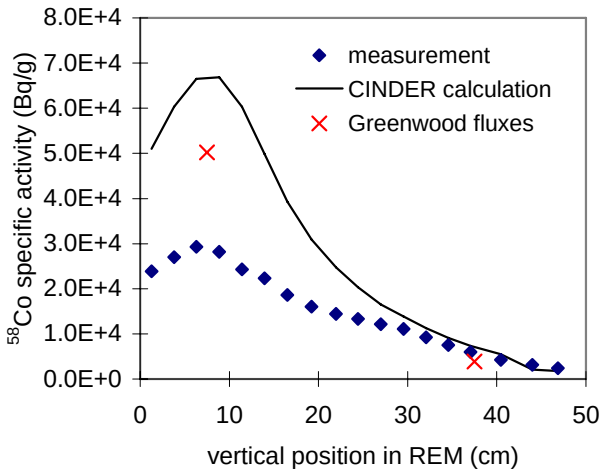

Figure 7. Specific activity of ^{58}Co at the time each wire segment was counted.

The ^{57}Ni activity was measured using the 1377.6-keV gamma ray. In this case we were able to count all the segments within the first few half-lives. Figure 8 shows a comparison between the calculated and measured values at the end of irradiation. As in the case of ^{58}Co, the ^{57}Ni activity peaks much more near the midplane of the target in the simulation than the measurement. The agreement at the upper end of the wire is also good although not quite as good as for ^{58}Co.

The ^{65}Ni activity was measured using the 1115.5- and 1481.9-keV gamma rays. Because of the very short half-life in this case, and the fact that the wire segments were initially too hot to count effectively, we have data only for the last two segments. Figure 9 compares the activity at the end of irradiation and shows that there is good agreement in this case between the measured and calculated values.

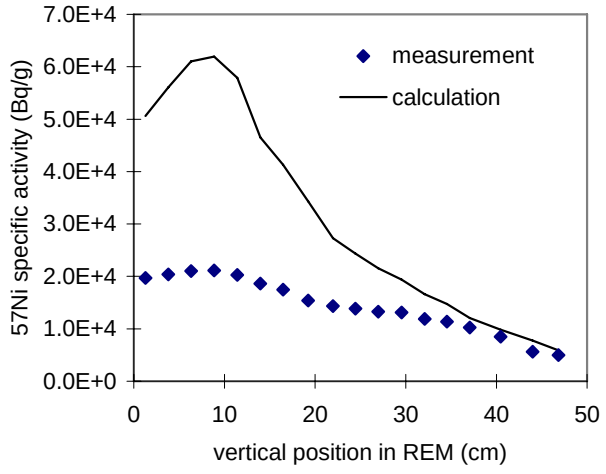

Figure 8. Specific activity of ^{57}Ni at the end of irradiation.

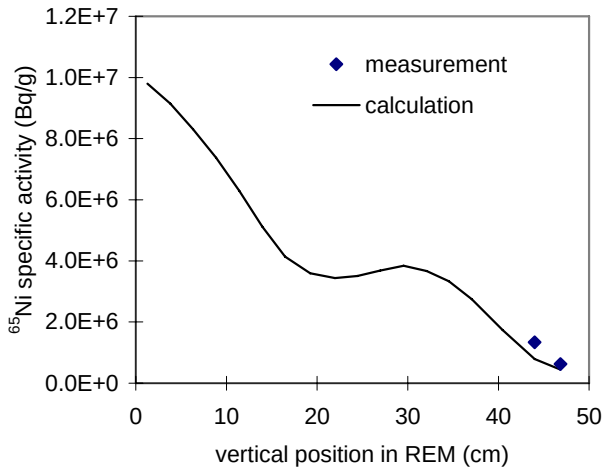

Figure 9. Specific activity of ^{65}Ni at the end of irradiation.

IV. BISMUTH SLUG MEASUREMENTS

IV.A. Bismuth Dosimetry Cross Sections

Bismuth is interesting in the context of fast neutron dosimetry since it is monoisotopic (Z = 83, A = 209) and the products of the (n,xn) reactions emit gamma rays which can be counted for values of n from 2 to 12. The cross sections for higher values of n have successively higher threshold energies, so that there is a possibility of using a single irradiated sample to measure neutron fluxes up to 100 MeV. The half-lives and principle gamma ray energies for selected bismuth isotopes are listed in Table III.

The ENDF and CINDER libraries contain cross sections only for the (n,2n) and (n,3n) reactions since the threshold energies for the (n,4n), etc. reactions are above the upper energy of the ENDF and CINDER cross section tables (20 and 25 MeV, respectively). These are shown in Figures 10 and 11. Maekawa [10] derived cross sections for ^{209}Bi(n,xn) reactions for values of x up to 12. Some of these are shown in Figures 11 and 12.

TABLE III. Half lives and principal gamma emissions from products of n+^{209}Bi reactions.

Reaction Product	Half-life	Principal Gamma Energies (keV)
^{203}Bi	11.8 h	820.3, 825.2, 897.0
^{204}Bi	11.2 h	374.8, 899.2, 984.0
^{205}Bi	15.31 d	703.4, 1718.7
^{206}Bi	6.243 d	516.2, 803.1, 881.0

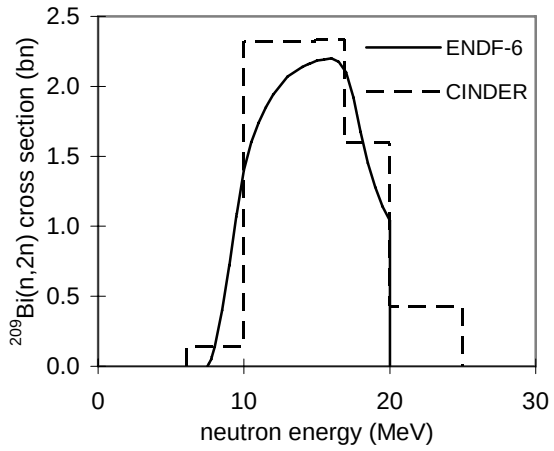

Fig. 10. Cross sections for the ^{209}Bi (n,2n) reaction.

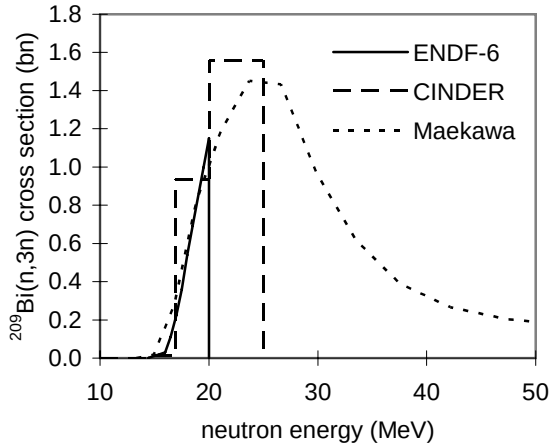

Fig. 11. Cross sections for the ^{209}Bi (n,3n) reaction.

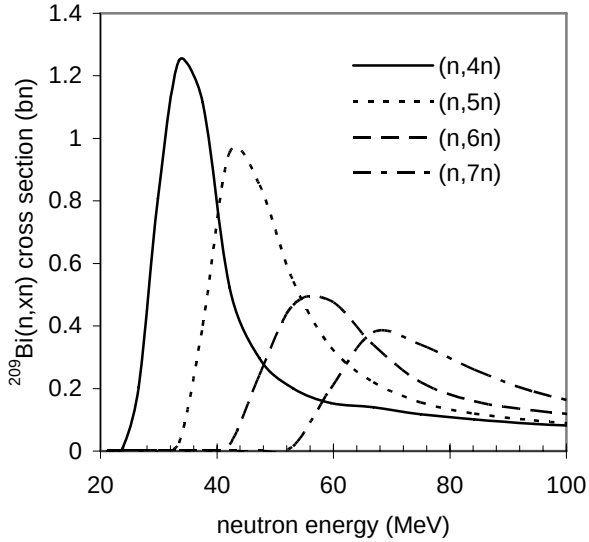

Fig. 12. Cross sections for the ^{209}Bi (n,4n), ^{209}Bi (n,5n), ^{209}Bi (n,6n), and ^{209}Bi (n,7n) reactions.

IV.B. Bismuth Slug Measurements

Bismuth slugs of dimension 1 cm high x 1 cm diameter were irradiated in the REM in the same positions as the foil packets were located in the Greenwood measurements. One set of slugs was irradiated for a short time (2 minutes) to focus on the short half-life nuclides ^{203}Bi and ^{204}Bi. A second set of slugs were irradiated for a longer time (6 days) to concentrate on the longer-lived ^{205}Bi and ^{206}Bi.

The resulting gamma activities were counted with a 50% HPGe detector and the spectra were analyzed with ORTEC's GammaVision software. Corrections were made for source geometry and self-attenuation of gamma rays inside the slugs using results of MCNPX simulations. Multiple gamma lines were analyzed for the activity of each product, with excellent agreement among the different gamma energies. Table IV shows the results averaged over the gamma lines analyzed.

The activities of these nuclides were calculated using the MCNPX and CINDER'90 codes as driven the activation script mentioned above. These calculated activities are also shown in Table IV. The calculated activities are higher than the measured ones, consistent with the fact that the MCNPX simulations yield higher neutron fluxes than the Greenwood foil data.

TABLE IV. Measured and simulated (CINDER) activities for products of n+^{209}Bi reactions.

irradiation time and location	product	measured activity (Bq)	calculated activity (Bq)
long-lower	^{206}Bi	3.7e+6	1.10e+7
	^{205}Bi	9.2e+5	3.04e+6
long-upper	^{206}Bi	1.7e+6	2.41e+6
	^{205}Bi	4.6e+5	7.28e+5
short-lower	^{204}Bi	4.5e+3	1.21+4
	^{203}Bi	2.9e+3	6.43e+3

We made another estimate of the activity of the nuclides listed in Table IV by combining the reaction cross sections of Maekawa with the neutron fluxes as measured by Greenwood and as calculated using MCNPX. While the Greenwood data were measured for the enriched uranium target, the neutron fluxes in the REM for E_n > 10 MeV do not depend on the degree of enrichment, as shown in Section II above. Therefore we can use these fluxes to estimate the rates for Bi(n,xn) reactions when using the depleted uranium target. These results are shown in Table V, along with the measured activity in the bismuth slugs. The MCNPX fluxes give higher (n,xn) reaction rates than the Greenwood fluxes, which is due to the higher fast flux. However, the

activities calculated using the Greenwood fluxes compare quite favorably with our measured activities.

TABLE V. Measured and simulated (CINDER) activities for products of n+^{209}Bi reactions.

irradiation time and location	measured activity (Bq)	calculated activity (Greenwood flux + Maekawa xs)	calculated activity (MCNPX flux + Maekawa xs)
long-lower			
^{206}Bi	3.7e+6	(4.25±0.95)e+6	(1.05±0.01)e+7
^{205}Bi	9.2e+5	(1.39±0.32)e+6	(3.11±0.04)e+6
long-upper			
^{206}Bi	1.7e+6	(1.10±0.27)e+6	(2.38±0.04)e+6
^{205}Bi	4.6e+5	(3.63±1.03)e+5	(7.62±0.14)e+5
short-lower			
^{204}Bi	4.5e+3	(5.6±1.6)e+3	(1.47±0.02)e+4
^{203}Bi	1.9e+3	(1.8±0.7)e+3	(7.95±0.14)e+3

V. CONCLUSIONS

Experimental irradiation data in the IPNS REM have been compared to the predictions of MCNPX simulations. These include earlier foil set measurements and more recent measurements made with nickel wires and bismuth slugs. In all cases, the fast neutron flux from the simulations show a large peak near the target which is not seen in the experimental data. Since the activities from the nickel wire and bismuth slug measurements agree well with reaction rates obtained from the neutron fluxes from the Greenwood foil measurements, we conclude that there is some inaccuracy in the MCNPX model of the IPNS target/reflector system which leads to an overprediction of the neutron flux. It is less likely that the physics models in MCNPX lead to an overprediction of the evaporation neutron yield. The neutron spectra from the Greenwood foil measurements can be adjusted for the difference between the enriched uranium and depleted uranium targets, and thus remain the most reliable means of estimating reaction rates in the REM, particularly for fast neutron-induced reactions.

ACKNOWLEDGMENTS

Argonne National Laboratory's work was supported by the U.S. Department of Energy, Office of Science, Office of Basic Energy Sciences, under contract DE-AC02-06CH11357. The IPNS Neutron Operations Group provided valuable support in executing the nickel wire and bismuth slug irradiations.

REFERENCES

1. W. B. WILSON et al., "Recent Developments of the CINDER'90 Transmutation Code and Data Library for Actinide Transmutation Studies," *Proc. GLOBAL'95 Int. Conf. on Evaluation of Emerging Nuclear Fuel Cycle Systems*, Versailles, France (Sept. 1995).
2. D. PELOWITZ, ed., "MCNPX User's Manual, Version 2.5.0," LA-CP-05-0369 (April 2005).
3. L. GREENWOOD, unpublished data, Argonne internal memo ACL#90-4047 (March 1990).
4. R. B. FIRESTONE and V. SHIRLEY, Eds., *Table of Isotopes, Eighth Edition*, Wiley-Interscience, New York, New York (1996).
5. "Radionuclide Transformations – Energy and Intensity of Emissions," *Annals of the ICRP*, **11-13** (1983).
6. V. AVRIGEANU et al., "Energy Dependence of the Isomeric Cross Section Ratio in the ^{58}Ni(n,p)^{58}Co^{m,g} Reactions," Phys. Rev. **C60**, 017602 (1999).
7. K. GUL, "Calculation of Excitation Functions and Isomeric Cross Section Ratio of the ^{58}Ni(n,p)^{58}Co^{m,g} Reactions in the 1-20 MeV Energy Range," Phys. Rev. **C62**, 067603 (1999).
8. V. SEMKOVA et al., "A Systematic Investigation of Reaction Cross Sections and Isomer Ratios for Neutrons up to 20 MeV on Ni-isotopes and ^{59}Co by Measurements with the Activation Technique and New Model Studies of the Underlying Reaction Mechanisms," Nucl. Phys. **A730**, 255-284 (2004).
9. F. GALLMEIER et al., "An Environment using Nuclear Inventory Codes in Combination with the Radiation Transport Code MCNPX for Accelerator Activation Problems," *Proc. of the Eighth Int'l Topical Meeting on Nuclear Applications and Utilization of Accelerators*, Pocatello, ID (Aug. 2007).
10. F. MAEKAWA, et al., "Production of a Dosimetry Cross Section Set Up to 50 MeV", *Proc. 10th International Symposium on Reactor Dosimetry*, Sept. 12-17, 1999, Osaka, Japan; ASTM STP 1398, pp. 417-424 (February 2001).